AJNR

This information is current as of July 21, 2025.

Application of a Denoising High-Resolution Deep Convolutional Neural Network to Improve Conspicuity of CSF-Venous Fistulas on Photon-Counting CT Myelography

Ajay A. Madhavan, Jeremy K. Cutsforth-Gregory, Waleed Brinjikji, John C. Benson, Felix E. Diehn, Ian T. Mark, Jared T. Verdoorn, Zhongxing Zhou and Lifeng Yu

Application of a Denoising High-Resolution Deep Convolutional Neural Network to Improve Conspicuity of CSF-Venous Fistulas on Photon-Counting CT Myelography

Ajay A. Madhavan, Jeremy K. Cutsforth-Gregory, Waleed Brinjikji, John C. Benson, Felix E. Diehn, Ian T. Mark, Jared T. Verdoorn, Zhongxing Zhou, and Lifeng Yu

ABSTRACT

SUMMARY: Photon-counting detector CT myelography is a recently described technique that has several advantages for the detection of CSF-venous fistulas, one of which is improved spatial resolution. To maximally leverage the high spatial resolution of photon-counting detector CT, a sharp kernel and a thin section reconstruction are needed. Sharp kernels and thin slices often result in increased noise, degrading image quality. Here, we describe a novel deep-learning-based algorithm used to denoise photon-counting detector CT myelographic images, allowing the sharpest and thinnest quantitative reconstruction available on the scanner to be used to enhance diagnostic image quality. Currently, the algorithm requires 4–6 hours to create diagnostic, denoised images. This algorithm has the potential to increase the sensitivity of photon-counting detector CT myelography for detecting CSF-venous fistulas, and the technique may be valuable for institutions attempting to optimize photon-counting detector CT myelography imaging protocols.

ABBREVIATIONS: CVF = CSF-venous fistula; CTM = CT myelography; HR-CNN = high-resolution deep convolutional neural network; PCCT = photon-counting detector CT; PC-CTM = photon-counting CT myelography; QIR = quantum iterative reconstruction; T3D = low-energy threshold

Photon-counting detector CT (PCCT) is an increasingly used imaging technology that has numerous benefits compared with traditional energy-integrating detector CT.[1,2] Some of the advantages of PCCT include improved spatial resolution, increased signal of contrast media, improved radiation dose efficiency, and inherent spectral imaging capabilities. These features result in improved diagnostic capabilities, reduction in radiation dose, and the ability to reduce doses of contrast media for some examinations.[3] Recently, PCCT myelography (PC-CTM) with the patient in the decubitus position was described as a technique to improve detection of CSF-venous fistulas (CVFs), a common cause of spontaneous intracranial hypotension.[2,4-6]

The improved spatial resolution conferred by PCCT is particularly helpful for detecting CVFs. PCCT has the capability of reconstructing images at a section thickness of 0.2 mm, whereas most modern energy-integrating detector CT scanners have a minimum section thickness of 0.5–0.6 mm or more. Because draining veins associated with CVFs are often near other densely opacified structures such as the thecal sac or meningeal

diverticula, high spatial resolution is sometimes necessary to make the diagnosis or increase diagnostic confidence.[6] To maximally leverage the high spatial resolution of PCCT, one must reconstruct images with a sharp kernel. If smoother kernels are used, spatial resolution is impaired. However, sharper-kernel reconstructions tend to introduce noise into the images, ultimately limiting the sharpness of the kernel that can be used without creating excessive noise. Here, we describe a novel deep-learning-based denoising algorithm used to improve the conspicuity of CVFs on PC-CTM. To our knowledge, this is the first application of such an algorithm in the realm of CT myelography, with prior algorithms having been used for chest imaging, CT angiography, and other applications.[7-9]

Technical Report

Background. The imaging protocol and technique for PC-CTM have been previously detailed.[6] Briefly, patients are placed in the decubitus Trendelenburg position on the PCCT table (NAEOTOM Alpha; Siemens), and 3–6 scans of the spine are obtained during active injection of 5 mL of Omnipaque 300 (GE Healthcare) after a lumbar puncture with a 22- or 20-ga spinal needle. Two of these scans are obtained in an ultra-high-resolution mode, permitting 0.2-mm section thickness recontructions. The needle is removed, and the process is repeated with the patient in the contralateral decubitus position after placing a new spinal needle. Initially, we reconstructed images using a low-energy threshold (T3D) and a
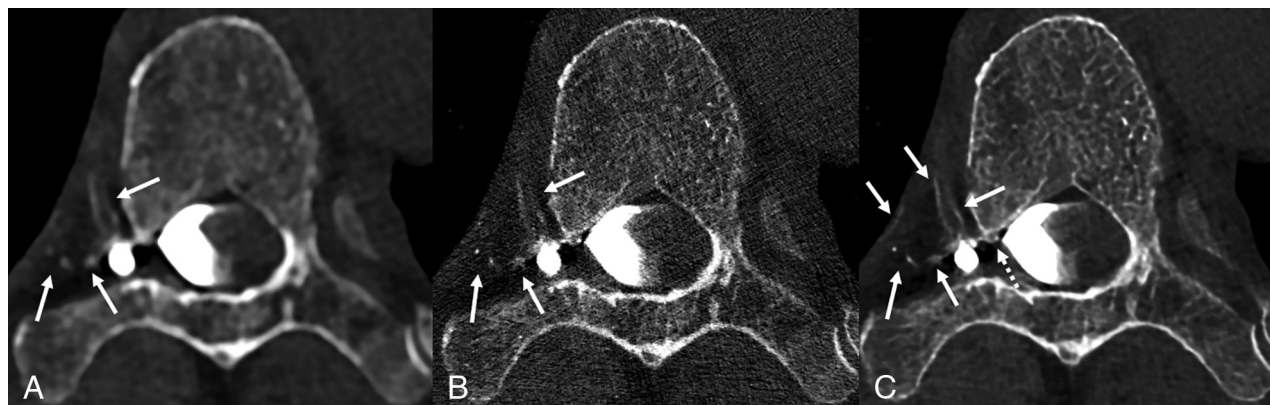
FIG 1. Axial low-energy thresholded (T3D) images in a 70-year-old man with a right T6 CVF. Images were reconstructed using a Br56 kernel (*A*), a sharper Qr89 kernel (*B*), and a Qr89 kernel after denoising with the trained model (*C*), all presented at the same section and window/level settings. Hazy opacification of the external vertebral venous plexus is evident using the smoother Br56 kernel (*A, arrows*). These external vertebral veins are poorly visualized using the Qr89 kernel secondary to noise (*B, arrows*). The denoised Qr89 image most clearly delineates all the involved veins, including multiple veins of the external vertebral venous plexus (*C, solid arrows*), and definite involvement of the internal vertebral venous plexus (*C, dashed arrow*).
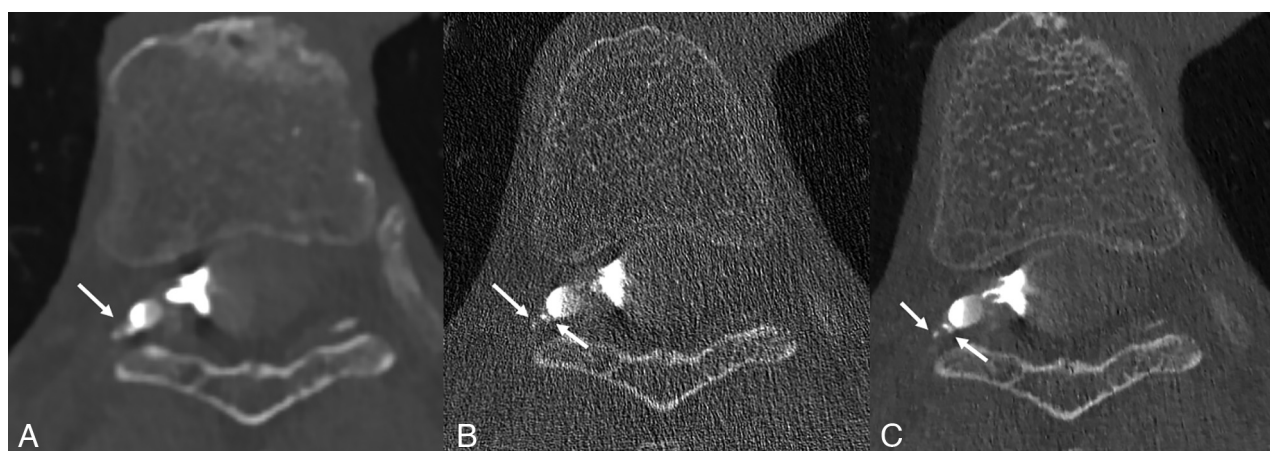
FIG 2. Axial low-energy thresholded (T3D) images in a 70-year-old woman with a right T7 CVF. Images were reconstructed using a Br56 kernel (*A*), a sharper Qr89 kernel (*B*), and a Qr89 kernel after denoising with the trained model (*C*), all presented at the same section and window/level settings. The Br56 kernel demonstrates ill-defined contrast lateral to a right T7 diverticulum (*A, arrow*), which was thought to be suspicious but not definitive for a CVF. The Qr89 kernel more clearly delineates this finding as likely venous opacification (*B, arrows*), though substantial noise degrades the overall image quality and results in uncertainty in the findings. The denoised Qr89 image clearly characterizes these structures as tiny veins, (*C, arrows*), confirming the presence of a CVF.

Br56 kernel at a quantum iterative reconstruction (QIR) strength of 4 (Figs 1*A*, 2*A*, and 3*A*). When a sharper Qr89 kernel was used, the resulting images were too noisy, impairing diagnostic performance (Figs 1*B*, 2*B*, and 3*B*).

Implementation of the Denoising Algorithm. Subsequently, we applied a deep-learning-based algorithm to denoise the Qr89 reconstructions. The denoising model was a dedicated high-resolution deep convolutional neural network (HR-CNN) that was trained using existing patient CT myelography (CTM) examinations acquired at a high-resolution mode and reconstructed with the Qr89 kernel and 0.2-mm section thickness.[8,9] Patient images were allocated into training/validation (7 patients) and testing (12 patients) data sets. The training/validation data set contained 11,115 routine-dose ultra-high-resolution spine CTM images reconstructed using both filtered back-projection and

QIR with strength 4 (QIR VA40; Siemens), which was split into training and validation sets using a 9:1 ratio. All images were reconstructed with the sharpest quantitative kernel (Qr89) and a pixel size of 0.15 mm (150-mm FOV and 1024 matrix) to fully use the high spatial resolution.

The following steps were used to generate paired input and target images for training the network. Noise maps were generated by taking the difference of thin-section filtered back-projection and iterative reconstruction images with section thickness/increment of 0.2/0.2 mm at the same anatomic location. Then the noise maps were scaled and random-translated with the range of -15 to $+15$ pixels. Iterative reconstruction images (0.4/0.2 mm) were reconstructed as the target images, while the input of the model was generated by adding the noise map to the corresponding target images.

FIG 3. Axial low-energy thresholded (T3D) images in a 50-year-old woman with a right T6 CVF. Images were reconstructed using a Br56 kernel (*A*), a sharper Qr89 kernel (*B*), and a Qr89 kernel after denoising with the trained model (*C*), all presented at the same section and window/level settings. The Br56 kernel demonstrates amorphous opacification around a right T6 diverticulum (*A, solid arrow*) and possible venous opacification in the internal vertebral venous plexus (*A, dashed arrows*). The Qr89 kernel more clearly delineates individual external vertebral veins (*B, solid arrow*), though the image is overall degraded secondary to noise (*B, dashed arrows*). The denoised Qr89 image clearly identifies all the involved veins, including the external vertebral veins (*C, solid arrow*) and ventral/dorsal internal vertebral venous plexus (*C, dashed arrows*).
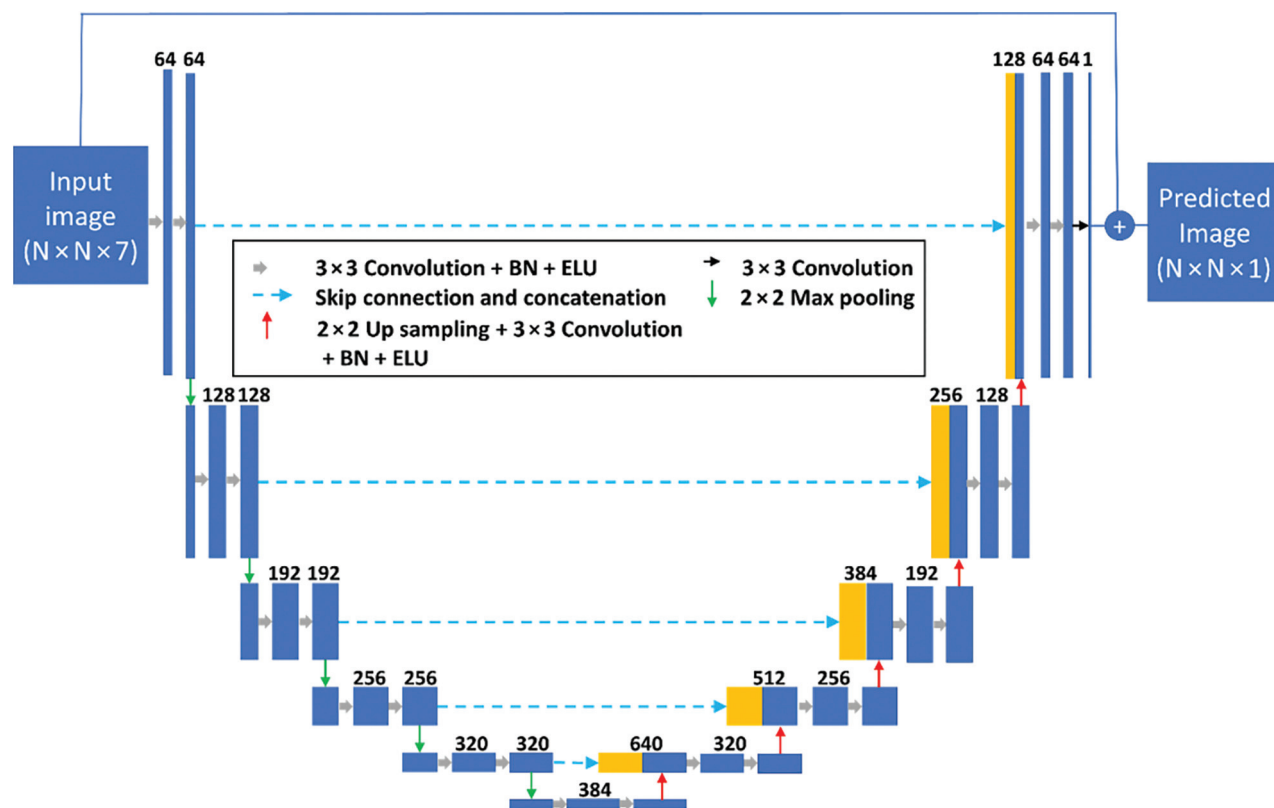
FIG 4. Schematic of the modified U-Net architecture used for this study. BN indicates batch normalization; ELU, exponential linear unit; N, arbitrary image size.

The proposed HR-CNN used a modified 6-layer residual U-Net as the architecture, (Fig 4). The architecture consists of 5 max pooling and up-convolutional layers, 64 filters with the number of filters increased by 64 at each pooling layer, and exponential linear unit activation. To optimize the performance of the HR-CNN model, we used 7 adjacent CT slices as the channel input of the model. The network was trained for 200 epochs using the Adam optimizer with a descending learning rate from 0.001 to 0.00001, and a minibatch of 16 image patches for each iteration. We used pixel-wise mean-squared-error between the HR-CNN

Characteristics of patients and CVFs to which the fully trained denoising algorithm was applied

Characteristics	
Total patients	12
No. female	8
Total number of CVFs	10 (1 CVF in each positive case)
No. right-sided CVFs	7
Levels of CVFs (No.)	T3 (2), T6 (2), T7 (1), T8 (3), T10 (1), T12 (1)
No. CVFs only visible on denoised images (occult on smooth B656 kernel or noisy Qr89 images)	5
No. CVFs visible on all series (Br56, Qr89, Qr89 denoised) but with improved diagnostic confidence and best visualization on denoised Qr89 images	5
No CVFs present	2

output and ground truth as the loss function during optimization. The training was performed on a Tesla M40 GPU (NVIDIA) with 12-GB memory. Training was performed by a CT physicist with special expertise in PCCT and 17 years of practice experience (L.Y.), as well as a postdoctoral fellow with subspecialty training in CT physics (Z.Z.).

With the fully trained model, we were able to input a 0.2-mm section thickness T3D series with a Qr89 kernel, resulting in an output series with the same spatial resolution but substantially decreased noise (Figs 1C, 2C, and 3C). The output series takes 4–6 hours to generate. In our early experience, the use of a sharp Qr89 kernel with denoising for PC-CTM has the potential to improve the conspicuity of veins draining CVFs. To date, the algorithm has been used in 12 patients. Specific preliminary data regarding the diagnostic utility of the algorithm in these 12 cases, on case review by a single neuroradiologist (A.A.M.), are available in the Table. The mean dose-length product for these 12 patients was 4572 mGy × cm for the full examinations, and 1242 mGy × cm for the ultra-high-resolution scans used to obtain the sharp kernel, denoised images.

DISCUSSION

Application of a deep-learning-based denoising algorithm resulted in substantial image-quality improvement on the sharpest quantitative kernel (Qr89) and thinnest section-thickness (0.2 mm) reconstructions during PC-CTM. The algorithm was successfully trained with 7 clinical PC-CTM ultra-high-resolution scans, with the potential for further improvement with more training data. On the basis of our preliminary experience, this algorithm has the potential to optimize the benefits of high spatial resolution on PC-CTM, which may lead to improved sensitivity and increased diagnostic confidence. Institutions using PC-CTM may benefit from using a denoising algorithm to permit image reconstruction with the sharpest kernel possible. Since this algorithm was developed, it is not currently publicly available, though ours or similar algorithms will likely become available in the near future. Further details regarding the specific algorithm, which can be used to denoise PC-CTM examinations and other examination types, are pending publication.[9]

Limitations of this preliminary technical report include the small number of examinations to which the algorithm has been applied ($n = 12$), the computer time taken to generate the denoised images with the algorithm (4–6 hours per examination), the potential cost for institutions seeking to incorporate similar algorithms (physicist time and computing resources), and the additional images requiring review (mean of 4020 added images per case requiring approximately 20 minutes to review in our patients). Furthermore, the clinical benefit of this algorithm remains to be demonstrated.

CONCLUSIONS

Specifically, future studies should focus on identifying how frequently the algorithm improves diagnostic confidence of CVFs on image review by neuroradiologists. Nonetheless, on the basis of our current experience, we believe that the algorithm will improve conspicuity of CVFs on PC-CTM and potentially even facilitate the diagnosis of otherwise missed CVFs.

REFERENCES

1. McCollough CH, Rajendran K, Leng S, et al. **The technical development of photon-counting detector CT.** *Eur Radiol* 2023;33:5321–30 CrossRef Medline
2. Schwartz FR, Malinzak MD, Amrhein TJ. **Photon-counting computed tomography scan of a cerebrospinal fluid venous fistula.** *JAMA Neurol* 2022;79:628–29 CrossRef Medline
3. Cundari G, Deilmann P, Mergen V, et al. **Saving contrast media in coronary CT angiography with photon-counting detector CT.** *Acad Radiol* 2023 July 31 [Epub ahead of print] CrossRef Medline
4. Schievink WI, Moser FG, Maya MM. **CSF-venous fistula in spontaneous intracranial hypotension.** *Neurology* 2014;83:472–73 CrossRef Medline
5. Pradeep A, Madhavan AA, Brinjikji W, et al. **Incidence of spontaneous intracranial hypotension in Olmsted County, Minnesota: 2019-2021.** *Interv Neuroradiol* 2023 Mar 22 [Epub ahead of print] CrossRef Medline
6. Madhavan AA, Yu L, Brinjikji W, et al. **Utility of photon-counting detector CT myelography for the detection of CSF-venous fistulas.** *AJNR Am J Neuroradiol* 2023;44:740–44 CrossRef Medline
7. VanMeter P, Marsh J Jr, Rajendran K, et al. **Quantification of coronary calcification using high-resolution photon-counting-detector CT and an image domain denoising algorithm.** *Proc SPIE Int Soc Opt Eng* 2022;12031:120311R CrossRef Medline
8. Huber NR, Ferrero A, Rajendran K, et al. **Dedicated convolutional neural network for noise reduction in ultra-high-resolution photon-counting detector computed tomography.** *Phys Med Biol* 2022;67 CrossRef Medline
9. Zhongxing Zhou AB, Chi Wan K, Kelly H, et al. **Pushing the limits of spatial resolution in clinical photon-counting-detector (PCD) CT using a dedicated high-resolution convolutional neural network (HR-CNN).** In: *Proceedings of the Annual Meeting of the Radiological Society of North America.* November 26–30, 2023. Chicago, Illinois